RESPONSE OF COMPOSITE PLATES WITH INCLINED ELLIPTICAL NOTCHES AND SUBJECTED TO AXIAL COMPRESSION

Damodar R. Ambur and David M. McGowan
NASA Langley Research Center
Hampton, Virginia 23681-0001

Presented at the AIAA/ASME/ASCE/AHS/ASC 40th Structures,
Structural Dynamics, and Materials Conference
St. Louis, MO
April 12-15, 1999

AIAA Paper No. 99-1276

AIAA Paper No. 99-1276

Response Of Composite Plates With Inclined Elliptical Notches and Subjected to Axial Compression

Damodar R. Ambur* and David M. McGowan†
NASA Langley Research Center
Hampton, VA

Abstract

An analysis method for predicting the inplane stress states in anisotropic finite plates with an elliptical notch is presented. This method can be used to analyze plates with arbitrary notch orientations with respect to the plate material axes. The analysis results have been validated using finite element analysis results for unnotched composite plates and experimental and finite element analysis results for stiffened composite panels with a skin that has orthotropic properties. The good agreement between these results, until the panel exhibits nonlinear response either due to bending or initiation of damage, indicates that the present analysis method can be used to determine accurately the inplane stress states and stress concentrations at and around an elliptical notch.

Introduction

Advanced composite materials are currently being considered for aerospace primary structural applications due to their potential for reduced structural weight. These structures have to be designed to operate safely in the presence of structural discontinuities such as holes and cracks. Current design and manufacturing practices require access holes for assembly and feed-through holes for cable and fuel lines. One of the damage tolerance criteria requires that the structure be qualified with a crack extending through two stiffener bays. The presence of structural discontinuities such as holes or cracks can degrade the strength and stiffness of these highly-loaded primary structures. Designing efficient structures requires a thorough understanding of the response of structures with stress concentrations that arise due to the presence of holes or cracks and subjected to combined inplane loading conditions.

Analytical solutions to determine stress concentrations around holes in anisotropic infinite plates were pioneered by Lekhnitski [1] and Savin [2] using a complex variable method developed by Mushkelishvili. However, no exact closed form solutions are available for determining stress concentrations in a finite anisotropic plate. Finite element analyses are the only methods available for obtaining stress distributions in finite composite plates. Since finite element analyses are computationally intensive, there is a need for developing other analysis methods which will enable the designer to evaluate the stress concentration problems more rapidly. Applying the concept of the Modified Mapping Collocation (MMC) technique introduced by Bowie and Neal [3], many researchers determined the stress intensity factors for cracks in rectangular orthotropic finite plates [e.g., 4,5]. Sampath and Hulbert [6] determined stress distributions in finite orthotropic laminates with multiple holes. They also investigated the stress concentrations around an inclined elliptical hole in a specially-orthotropic laminated plate. Ogonowski [7] employed the complex variable technique in conjunction with the boundary collocation method to determine the stress concentrations around a circular hole in a finite laminated plate. Lin and Ko [8] employed the same boundary collocation technique to determine the stress concentrations and strength predictions for finite composite plates with elliptical holes.

There is no analysis method available which has been thoroughly validated using either finite element

* Assistant Head, Structural Mechanics Branch. Associate Fellow, AIAA.
† Aerospace Engineer, Structural Mechanics Branch. Senior Member, AIAA.

analysis or experimental results to determine stress distributions around an inclined narrow elliptical notch in finite anisotropic plates subjected to combined inplane loading conditions. The objective of the present paper is to present and discuss a validated analysis procedure which can be used to determine stress concentrations and stress and strain distributions around a narrow elliptical notch in finite anisotropic composite laminated plates and three-stiffener panels loaded in axial compression. The present analysis method was validated by comparing the analytical stress and strain results with finite element analysis results for square laminated plates with notches oriented in two different angles to the loading direction. The present analysis results and finite element analysis results are also compared with the experimental results for three-stiffener panels with long elliptical notches.

Analysis Approach

This section outlines the governing equations, boundary conditions and solution procedure for a finite anisotropic plate that has an inclined elliptical notch and is subjected to in-plane loads applied along its outer edges. The method of analysis is based on (a) classical lamination plate theory, (b) anisotropic theory of elasticity, and (c) least-squares boundary collocation approximation procedure. The geometry and coordinate systems used in this study are shown in Fig. 1. The plate has a thickness h, length L and width w. The analysis method is derived for the general case of an elliptical hole having a semi-major axis 'a' and semi-minor axis 'b'. The principal axes of the ellipse are oriented at an angle α to the material axes x and y of the plate.

For plane stress problems, the solution is fully defined by the stresses σ_x, σ_y, and τ_{xy}. In a laminated composite plate, the in-plane stress resultants and the strains are related by

$$\begin{Bmatrix} N_x \\ N_y \\ N_{xy} \end{Bmatrix} = \begin{bmatrix} A_{11} & A_{12} & A_{16} \\ A_{12} & A_{22} & A_{26} \\ A_{16} & A_{26} & A_{66} \end{bmatrix} \begin{Bmatrix} \varepsilon_x \\ \varepsilon_y \\ \varepsilon_{xy} \end{Bmatrix} \tag{1}$$

Where

$$A_{ij} = \sum_{k=1}^{N} \bar{Q}^{(k)}_{ij} h_k \tag{2}$$

in which $\bar{Q}^{(k)}_{ij}$ are the reduced stiffnesses and h_k is the thickness of the kth layer. For practical convenience, the composite laminate is considered as a homogenous anisotropic single layer. On combining equilibrium and compatibility equations and introducing the Airy stress function U(x,y), which is related to the stresses as

$$\sigma_x = \frac{\partial^2 U}{\partial y^2}, \sigma_y = \frac{\partial^2 U}{\partial x^2}, \tau_{xy} = \frac{\partial^2 U}{\partial x \partial y} \tag{3}$$

the resulting field equation can be expressed as

$$S_{22}\frac{\partial^4 U}{\partial x^4} \pm 2S_{26}\frac{\partial^4 U}{\partial x^3 \partial y} + (2S_{12} + S_{66})\frac{\partial^4 U}{\partial x^2 \partial y^2} \pm 2S_{16}\frac{\partial^4 U}{\partial x \partial y^3} + S_{11}\frac{\partial^4 U}{\partial y^4} = 0 \tag{4}$$

where S_{ij} are laminate compliance coefficients and are equal to $[A_{ij}]^{\pm 1}$. The general expression for the stress function U(x,y) depends on the roots of the characteristic equation associated with the biharmonic equation and is given as

$$S_{11}\mu^4 \pm 2S_{16}\mu^3 + (2S_{12} + S_{66})\mu^2 \pm 2S_{26}\mu + S_{22} = 0 \tag{5}$$

Lekhnitski [1] has shown that Equation (5) has no real roots. In general, these roots are not equal and can be represented by two pairs of complex conjugate roots and are given as μ_1, $\bar{\mu}_1$, μ_2, and $\bar{\mu}_2$. Since the stress function is real, the stress function is expressed as

$$U = 2\,\mathrm{Re}[U_1(Z_1) + U_2(Z_2)] \tag{6}$$

where $U_1(Z_1)$ and $U_2(Z_2)$ are analytic functions of the complex variables $Z_1 = x + \mu_1 y$ and $Z_2 = x + \mu_2 y$, respectively. Introducing these functions, the general expressions for stress and displacement components can be written as

$$\begin{aligned} \sigma_x &= 2\mathrm{Re}\,[\mu_1^2 \varphi_1'(Z_1) + \mu_2^2 \varphi_2'(Z_2)] \\ \sigma_y &= 2\mathrm{Re}\,[\varphi_1'(Z_1) + \varphi_2'(Z_2)] \\ \tau_{xy} &= \pm 2\mathrm{Re}\,[\mu_1 \varphi_1'(Z_1) + \mu_2 \varphi_2'(Z_2)] \\ u &= 2\mathrm{Re}\,[p_1 \varphi_1(Z_1) + p_2 \varphi_2(Z_2)] \\ v &= 2\mathrm{Re}\,[q_1 \varphi_1(Z_1) + q_2 \varphi_2(Z_2)] \end{aligned} \tag{7}$$

where

$$p_1 = S_{11}\mu_1^2 + S_{12}$$
$$p_2 = S_{11}\mu_2^2 + S_{12}$$
$$q_1 = S_{12}\mu_1 + \frac{S_{22}}{\mu_1}$$
$$q_2 = S_{12}\mu_2 + \frac{S_{22}}{\mu_2}$$

The functions $\varphi_1(Z_1)$ and $\varphi_2(Z_2)$ are determined by satisfying the boundary conditions. An appropriate choice of these functions for a particular problem considerably simplifies computational details and speeds up the convergence to an accurate solution. The finite plate with a hole is considered as a doubly-connected region whose outer boundary is rectangular and inner boundary is elliptic or circular. For such a doubly connected region, the unknown functions can be expressed in terms of the Laurent series expansion as

$$\varphi_k(Z_k) = A_k \ln Z_k + \sum_{n=\pm\infty}^{\infty} B_{kN} Z_k^N \quad (k = 1,2) \tag{8}$$

The $\ln Z_k$ term is present whenever the resultant of the applied forces on the internal boundary is non-zero (i.e., a loaded hole). The coefficients A_k are determined by imposing the conditions of single valuedness to the displacements. The coefficients A_k are equal to zero for an unloaded hole.

The Laurent series expansion for the unknown functions yields a converged solution only for points in the complex plane that are a distance greater than or equal to a unit radius from the origin. The primary complex plane must be conformally mapped onto the exterior of a unit circle on a parametric plane to obtain converged results. A wide variety of problems can be solved once the conformal mapping solution is determined for the internal boundary.

The procedure for determining the mapping function is given in Refs. 1 and 2. For a plate with an elliptical hole with semi-major and semi-minor axes a and b respectively, coinciding with x and y directions, the mapping functions are given by

$$\xi_k(Z_k) = \frac{Z_k + \sqrt{Z_k^2 \pm (a^2 + \mu_k^2)}}{(a \pm i\,\mu_k\, b)} \quad (k = 1,2) \tag{9}$$

Since the principal axes of the ellipse are oriented at an angle α with respect to the principal material directions, the parametric equation of the ellipse are

$$x' = a\cos\theta \quad y' = b\sin\theta \tag{10a}$$
$$x = x'\cos\alpha \pm y'\sin\alpha \quad y = x'\sin\alpha + y'\cos\alpha \tag{10b}$$

where θ is measured in the x' and y' coordinate system. Substitution of equation (10a) into equation (10b) results in

$$x = a\cos\alpha\cos\theta \pm b\sin\alpha\sin\theta$$
$$y = a\sin\alpha\cos\theta + b\cos\alpha\sin\theta \tag{11}$$

Using the x and y values from equation (11), the mapping function given in equation (9) becomes

$$\xi_k(Z_k) = \frac{Z_k + \sqrt{Z_k^2 \pm \left\{a^2\pi_1 + b^2\pi_2\right\}}}{a\pi_3 \pm i\,b\pi_4} \quad (k = 1,2) \tag{12}$$

$$\pi_1 = (\cos^2\alpha + \mu_k^2\sin^2\alpha + \mu_k\sin 2\alpha)$$
$$\pi_2 = (\sin^2\alpha + \mu_k^2\cos^2\alpha \pm \mu_k\sin 2\alpha)$$
$$\pi_3 = (\cos\alpha + \mu_k\sin 2\alpha)$$
$$\pi_4 = (\mu_k\cos\alpha \pm \sin\alpha)$$

Equation (12) can be used as the mapping function for inclined cracks, where the crack is modeled as an elongated ellipse.

The B_{kN} coefficients of the Laurent series expansion are determined by a least-squares boundary collocation technique [Ref. 6-8]. This determination is accomplished by limiting the infinite series expansion of the stress function to a finite number of positive and negative terms. A set of uniformly spaced points is selected for the plate and hole boundaries, and the boundary conditions are satisfied at these selected points. The number of equations for the boundary conditions is greater than the number of terms retained for the series. A value for the ratio of the number of equations to the number of terms of 1.5 to 3.0 is suggested in Ref. 6. The over-determined system of equations is represented by the generalized matrix form

$$A\,X = B \tag{13}$$

where A denotes the matrix of coefficients from the truncated series and B is the vector of boundary conditions. The over-determined system of simultaneous linear equations is then solved for the unknown

coefficients by minimizing the average squared error of the boundary conditions. This solution can be expressed in a matrix form as

$$A^T A X = A^T B \tag{14}$$

where the superscript T denotes the transpose of a matrix. Once the coefficients of the series are calculated, stresses can be determined at any point in the plate. The truncated Laurent series for the present study has 23 negative terms and 17 positive terms. Eighty boundary points were selected for the elliptical hole boundary and 20 boundary points were selected for each side of the rectangular plate. The choices for the number of terms in the truncated series and number of boundary collocation points led to convergence for all the results presented herein.

Specimen Description and Test Conditions

Experimental results from two multi-stiffener panels have been used to compare with the present analysis results. These specimens were made from the Hercules Inc., AS4/3502 graphite-epoxy material system. The skin and stiffeners of this panel are made from stacks of this material, which were stitched together and resin film infiltrated to form a three-stiffener panel shown schematically in Fig. 2. Nominal values for the mechanical properties for each stack of this material are provided in Table 1. Each stack of material is 0.058 inches thick and is composed of 7 plies with a stacking sequence of $[45,-45,0,\overline{90}]_s$. The thicknesses of the plies are 0.00633, 0.01285, and 0.007018 inches for ±45, 0, and 90-degree orientations, respectively. The notch is typically 0.19-in. wide and 7-in. long and is machined across the panel width through the center stiffener either at 90° or at 30° to the axial loading direction. Both composite panels are stringer-stiffened panels that were machined from the upper and lower cover of a 12-foot-long, stitched graphite-epoxy wing box manufactured by the Boeing Company (formerly McDonnell Douglas) as part of the NASA Advanced Composites Technology (ACT) program. A complete description of this wing box is given in Ref. 9. The panels were loaded in uniaxial compression. The loaded ends of the panels were encased in 1.5 inches of epoxy potting compound to prevent an end-brooming failure, and the unloaded edges of the panel were supported with knife-edge supports to provide a simple support boundary condition along those edges. A photograph of the test set-up for these panels is given in Fig. 3. The electrical resistance strain gages used for monitoring the inplane strains are also identified in the figure.

Results and Discussion

The results of the present study are presented in two parts. In the first part, the present analysis method is validated by comparing the inplane stress results from the literature and finite element analysis results for finite plates with arbitrarily oriented narrow elliptical notches. In the second part, the present analysis results are compared with finite element analysis and experimental stress results for three-stiffener panels with long and narrow notches oriented along two different directions to the loading axis.

Validation of the present analysis method using finite element analysis results

To validate the analysis procedure, a computer code was written in FORTRAN 77 and implemented. The case of an inclined narrow elliptical hole in a specially orthotropic square plate as given in Ref. 6 was solved and the results are compared with results from the present analysis in Fig. 4. The stress magnitudes around the crack radius are normalized with respect to the far field stress and these values are plotted as a function of θ in degrees (Fig. 1) to represent the stress concentrations. The results obtained using the present analysis method compare very well with results in Ref. 6.

A composite plate which is representative of a skin on a wing cover panel is considered next. This plate is 12-in. square and is clamped along all of the edges. This plate consists of eight stacks of AS4/3501-6 graphite-epoxy material. Nominal values for the mechanical properties of this material are provided in Table 1. Each stack of material is 0.058 inches thick and is composed of 7 plies with a stacking sequence of $[45,-45,0,\overline{90}]_s$. The thicknesses of the plies are 0.00633, 0.01285, and 0.007018 inches for ±45, 0, and 90 degree orientations, respectively. The typical notch is 0.19-in. wide and is 7-in. long.

The finite element analysis of the plate is conducted using the Structural Analysis of General Shells (STAGS) code [10]. The finite element analysis results for a case where the notch is inclined at 90° (α=90°) to the loading direction is presented in Fig. 5. The axial stress contours shown in Fig. 5(a) indicate that the stress concentration is at θ=0°. The axial stress magnitudes from the finite element analysis results presented in Fig. 5(b) compare very well with the present analysis results presented in Fig. 5(c). The next case considered has the notch inclined at an angle of α=60°. The axial stress results from the finite

element analysis presented in Figure 6(a) suggest that the stress concentration occurs at $\theta>0°$. The locations and magnitudes for the stress concentration predicted from the two analyses are shown in Figs. 6(b) and 6(c) which indicate good correlation.

The strain distributions along a line passing through the location of axial stress concentration is presented in Fig. 7 for notches inclined at $\alpha=90°$ and $\alpha=60°$. These results are plotted as a function of the distance from the crack tip, R (see Fig. 1). The axial, transverse, and shear strain results from the finite element analysis and the present analysis compare very well for the range of R values shown in the figure. Compared to the case with $\alpha=90°$, the axial strain magnitude decreases and the shear strain magnitude increases as the magnitude of the crack orientation angle is changed to 60°. This change in stress state in the vicinity of the crack tip suggests that the location of damage initiation and the damage modes at the crack tip could be influenced by changes in the crack orientation angle. These results indicate that the present analysis method is adequate for predicting the location and magnitude of the stresses and strains in composite plates with arbitrarily oriented narrow elliptical notches.

Three-stiffener compression panel results

Two three-stiffener panels have been tested with notch inclination angles of 90° and 60°. A typical panel configuration is shown in Fig. 2. A finite element model of the test panel is shown in Fig. 8(a) together with the finite element discretization in the vicinity of the notch tip in Fig. 8(b). To determine the stress state in the notch-tip region with the present analysis method, the far field axial compressive stress for the three-stiffener panel needs to be determined first. When the panel has no out-of-plane deformations, the total panel load is distributed between the skin and the stiffeners in a direct proportion to their inplane stiffnesses. The presence of the notch does not influence the far-field load distribution in a long panel. The far-field axial strains that are calculated using the far-field axial stresses are compared with the experimentally measured axial strain results in Fig. 9. These results suggest that the far-field strain predictions compare very well with the experimental results up to the point where either the out-of-plane deformations or damage initiation at the notch tip cause load redistribution. The far-field stresses estimated analytically have been used to assess the influence of notch angle on the stress distributions around the notch tip for the two panels.

The variation of axial strains at the notch tip for the three-stringer panel with a 90° notch is presented in Fig. 10 as a function of the far-field stress. The experimental results for the axial strain at a point that is 0.1-in. away from the notch tip are presented and compared with the finite element results and the present analysis results. The experimental results suggest that a non-linearity exists in the response for far-field compressive stress values greater than approximately 10,000 psi, and this nonlinear response is not captured by the finite element analysis results. Since geometrically nonlinear finite element analysis was performed to predict the panel stress states, this departure in the experimental results from the finite element analysis results is attributed to the initiation of failure at the notch. Damage initiation is not included in the finite element analysis. The present analysis results differ from the experimental results by a maximum of 18 percent until damage initiates in the panel. The experimental lateral strain results for this test case have not been measured and, hence, are not presented here; the shear strain value at the notch tip for this panel configuration is zero.

The experimental and analytical strain results for the panel with a 60° notch angle are presented in Fig. 11. These results are compared at a point that is 0.25-in. away from the notch tip. All inplane strain components have non-zero values for the case with a 60° notch orientation. The presence of a combined stress state due to the application of a uniaxial compression load suggests that the principal stress orientations are inclined to the specimen coordinate axes. Damage initiation for this test case has been observed to occur along a plane that is inclined to the mid-section of the panel (Ref. 11). The axial, lateral, and shear strain results presented in Fig. 11 (a-c) indicate that the panel response becomes nonlinear at a far-field stress value of approximately 7,000 psi. The finite element analysis results compare very well with the experimental results until the far-field stress value reaches this level. The axial, lateral, and shear strain results from the present analysis are within 10 percent of either the experimental or the finite element analysis results. The finite element results or the experimental results are based on strain values that are smeared over an area that is a distance away from the semi-circular tip of a slit. The present analysis results are obtained at a point in a high strain gradient region along the major axis of a narrow elliptical notch. In view of these differences, comparisons between the present analysis results and the test results are very good. The present analysis method is a good preliminary analysis tool to predict the stress concentrations around an arbitrarily oriented notch. The strain information obtained in this

manner can be used to predict damage initiation at a notch tip.

Concluding Remarks

An analysis approach to determine the inplane stress states at the tip of a narrow elliptical notch in an anisotropic plate was presented. This analysis approach can be used to analyze plates with arbitrarily oriented notches and are subjected to combined inplane loading conditions. The results from this present analysis approach are compared with results from the open literature, finite element analysis results presented in this paper for laminated composite plates, and finite element analysis and experimental results for three-stiffener panels loaded in axial compression. The present analysis results, finite element analysis results, and experimental results are in very good agreement for the panels studied until the panels begin to exhibit nonlinear response. Geometric nonlinearities and the nonlinearities due to damage initiation and growth are not included in the present analysis. The correlation between the results suggest that the present analysis method can be used to determine stress states in laminated composite plates with narrow elliptic notches and to assess damage initiation for different inplane loading conditions. This method also provides a verified analysis tool for designing composite structures with narrow elliptic and circular cutouts.

References

1. Lekhnitskii, S. G., Anisotropic plates, Gordon and Breach Science Publishers, New York, 1968.
2. Savin, G.N., Stress Concentrations Around Holes, Pergamon Press, London, 1961.
3. Bowie, O. L. and Neal, D. M., "A Modified Mapping Collocation Technique for Accurate Calculation of Stress Intensity Factors," International Journal of Fracture Mechanics, Vol. 5, No. 6, March 1970, pp. 199-206.
4. Bowie, O. L. and Freese, C. E., "Central Crack in Plane Orthotropic Rectangular Sheet," International Journal of Fracture Mechanics, Vol. 8, No. 1, March 1972, pp. 49-58.
5. Gandhi, K. R., "Analysis of an Inclined Crack Centrally Placed in an Orthotropic Rectangular Plate," Journal of Strain Analysis, Vol. 7, No. 3, 1972, pp. 157-162.
6. Sampath, S. G. and Hulbert, L. E., "Analysis of Multiholed Orthotropic Laminated Plates by the Boundary-Point-Least-Squares Method," Journal of Pressure Vessel Technology, Transactions of the ASME, May 1975, pp. 118-122.
7. Ogonowski, J. M., "Analytical Study of Finite Geometry Plates with Stress Concentration," Proceedings of 21st AIAA/ASME/ASCE/AHS Conference, May 12-14, 1980, Seattle, Washington, pp. 694-698.
8. Lin, C. C. and Ko, C. C., "Stress and Strength Analysis of Finite Composite Laminates with Elliptical Holes," Journal of Composite Materials, Vol. 22, April 1988, pp. 373-385.
9. Jegley, D. C. and Bush, H. G., Structural Test Documentation and Results for the McDonnell Douglas All-Composite Wing Stub Box, NASA TM 110204, April 1997.
10. Brogan, F. A., Rankin, C. C. and Cabiness, H. D., "STAGS User Manual," Lockheed Palo Alto Research Laboratory Report LMSC P032594, 1994.
11. Davila, C.G., Ambur, D. R., and McGowan, D. M., "Analytical Prediction of Damage Growth in Notched Composite Panels Loaded in Axial Compression," AIAA-99-1435, April 1999.

Table 1. Typical mechanical properties for the stitched/RFI graphite-epoxy material systems.

Property	AS4/3501-6	AS4/IM7/3501-6
E_x, Msi	8.17	9.98
E_y, Msi	4.46	4.45
G_{xy}, Msi	2.35	2.57
V_{xy}	0.458	0.409

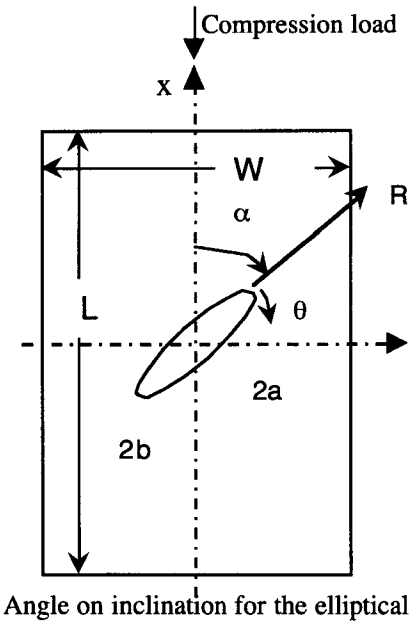

α: Angle on inclination for the elliptical notch.
θ: Angular position from the elliptical notch major axis.
R: Distance from the notch tip in inches

Figure 1. Plate and notch geometry, dimensions, and coordinate system.

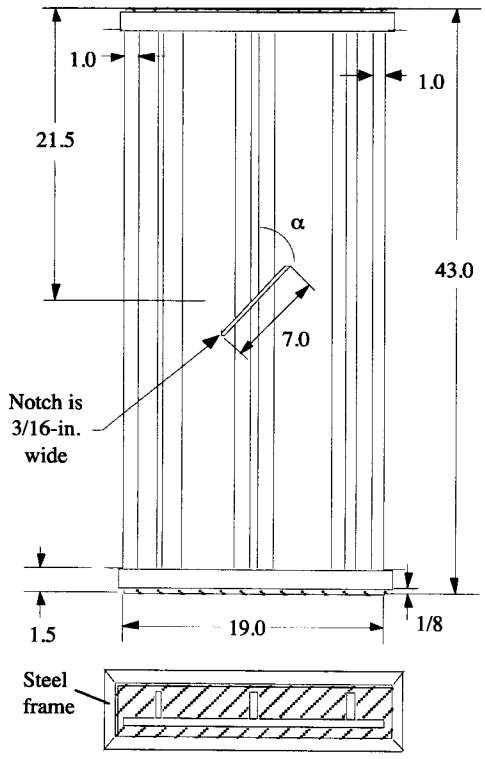

Figure 2. Schematic of the stitched, graphite-epoxy panel with a centered, machined notch through the center stringer (dimensions are in inches).

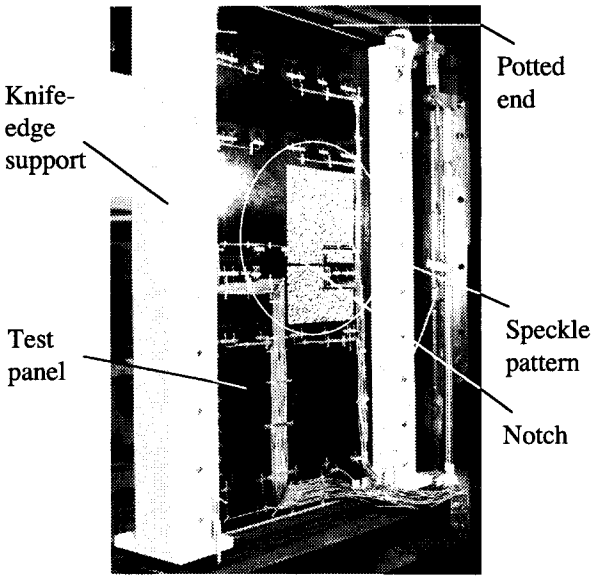

Figure 3. Photograph of the panel test setup.

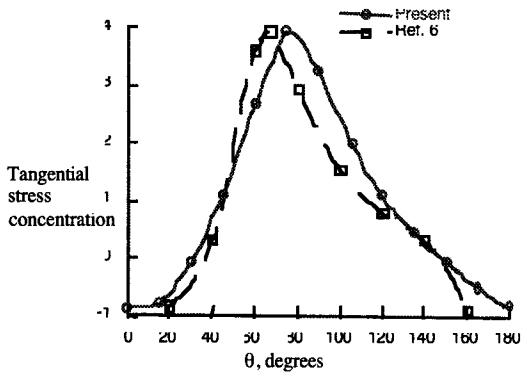

Figure 4. Comparison of analytical stress results around an elliptical notch inclined at 45° to the loading direction in a specially orthotropic square plate.

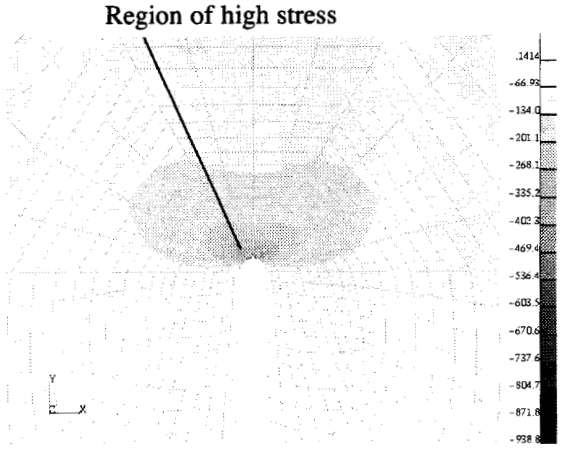

a. Finite element mesh and location of stress concentration

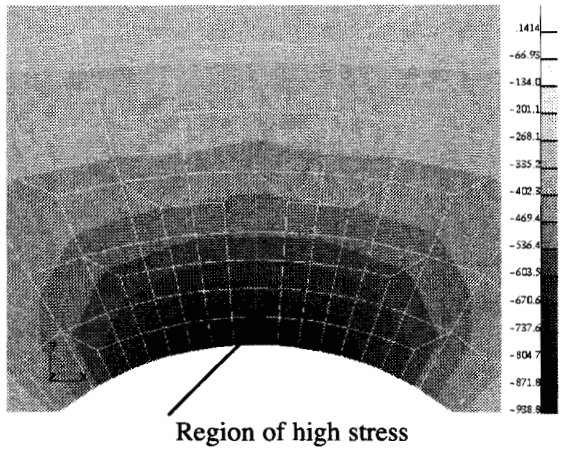

b. Enlarged view of stress contours from finite element analysis results

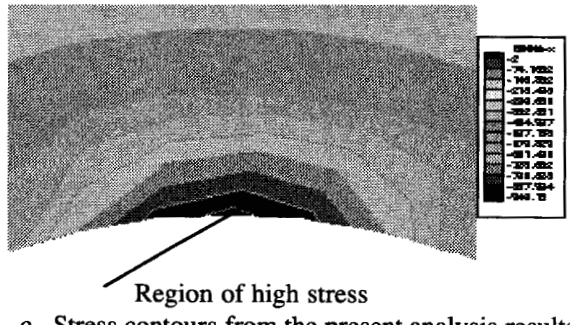

c. Stress contours from the present analysis results

Figure 5. Comparison of axial stress results from the finite element and present analyses in the vicinity of an elliptical notch oriented at $\alpha = 90°$ in an axially compressed composite plate.

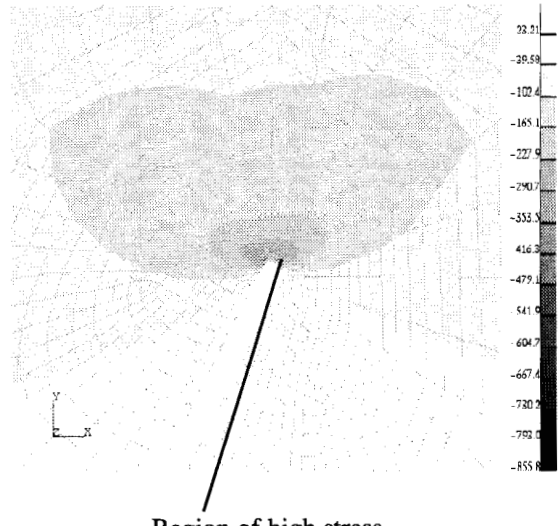

a. Finite element mesh and location of stress concentration

Figure 6. Comparison of axial stress results from finite element and present analyses in the vicinity of an elliptical notch oriented at $\alpha = 60°$ in an axially compressed composite plate.

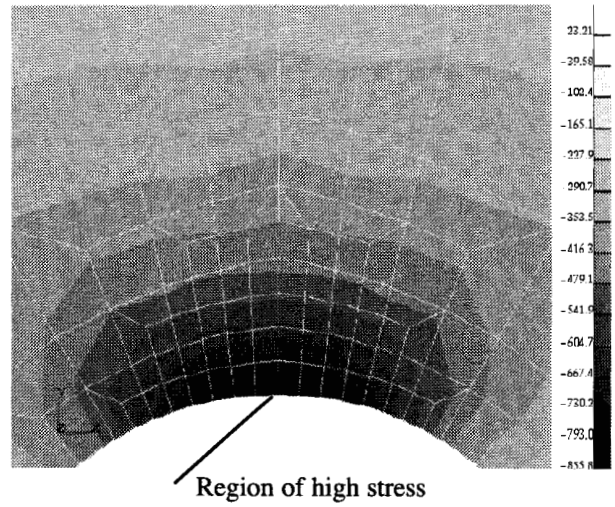

b. Enlarged view of stress contours from finite element analysis results

Figure 6. Continued.

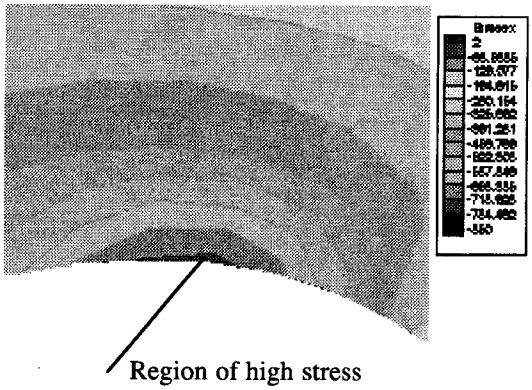

c. Stress contours from present analysis results

Figure 6. Concluded.

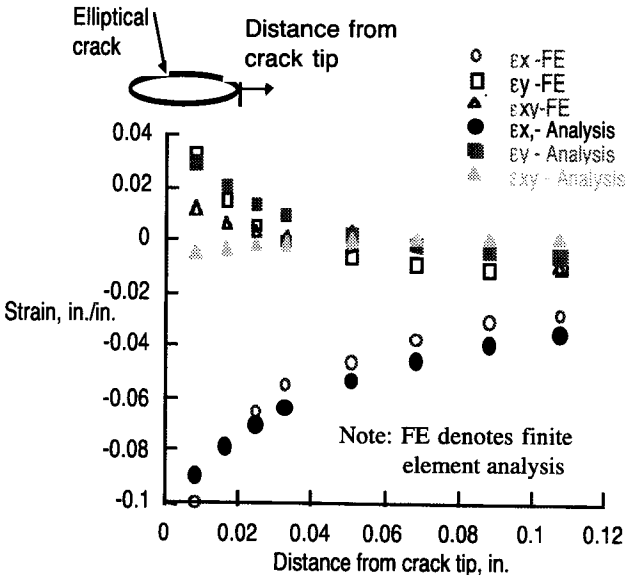

a. Elliptical notch oriented at α =90°

Figure 7. Continued.

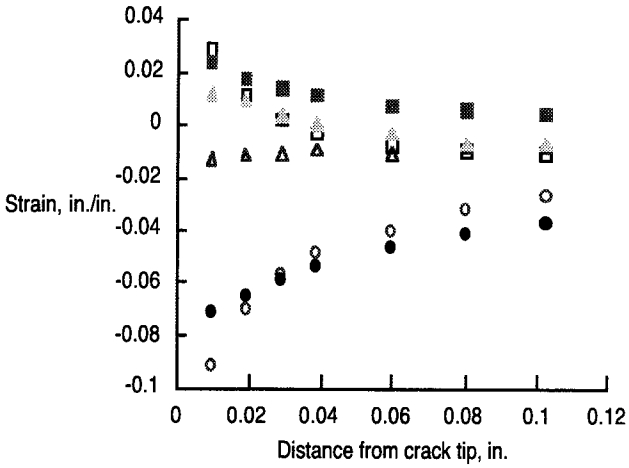

b. Elliptical notch oriented at α=60°

Figure 7. Comparison of inplane strain results from the finite element analysis and present analysis.

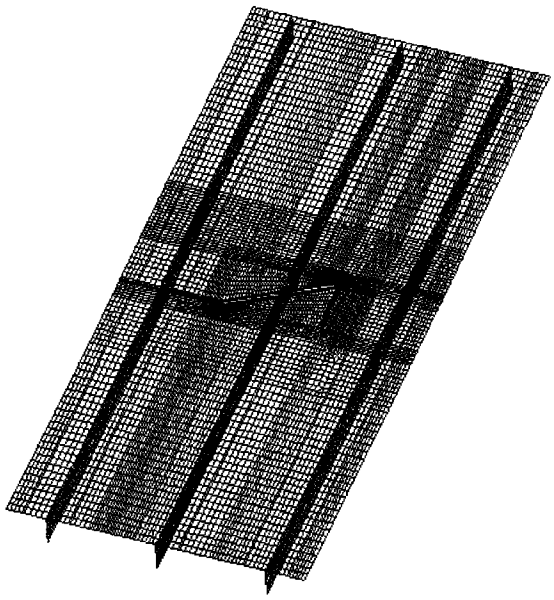

a. Panel model

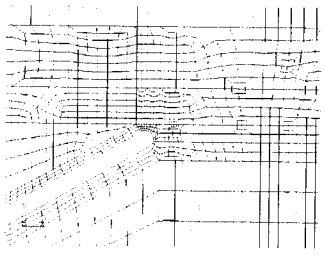

b. Mesh detail at the notch tip

Figure 8. Finite element model of the three-stiffener panel with a 60° notch.

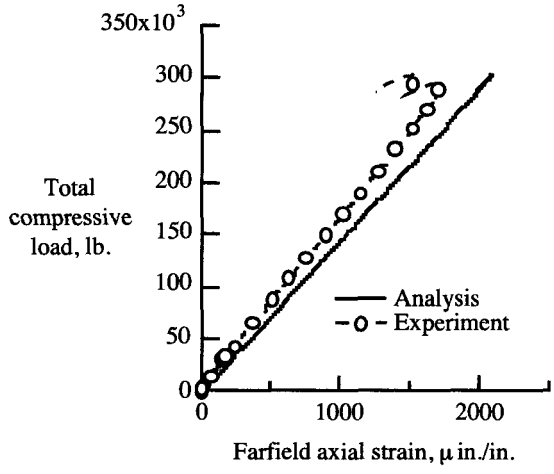

Figure 9. Comparison of experimental and analytical far-field axial strain results for the skin.

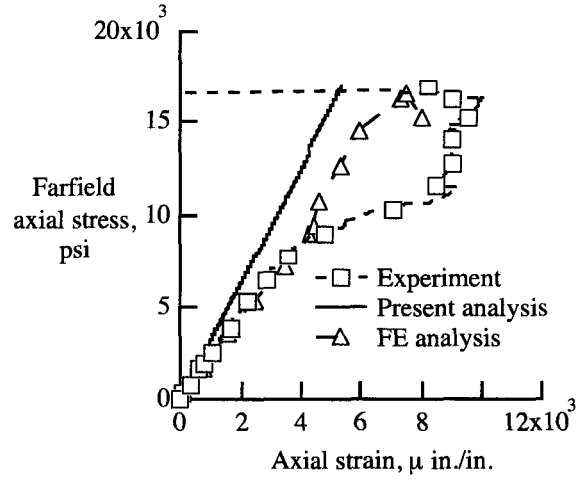

a. Axial strain results

Figure 11. Comparison of experimental and analytical axial strain results at a point 0.25-in. away from the notch tip for a three-stiffener panel with a 60° notch.

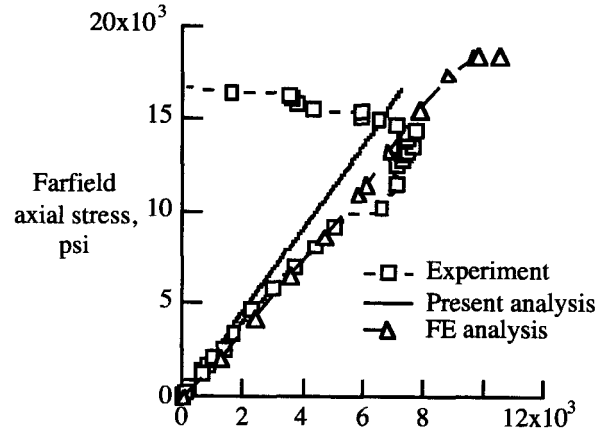

Figure 10. Comparison of experimental and analytical strain results at a point 0.1-in. away from the notch tip for a three-stiffener panel with a 90° notch.

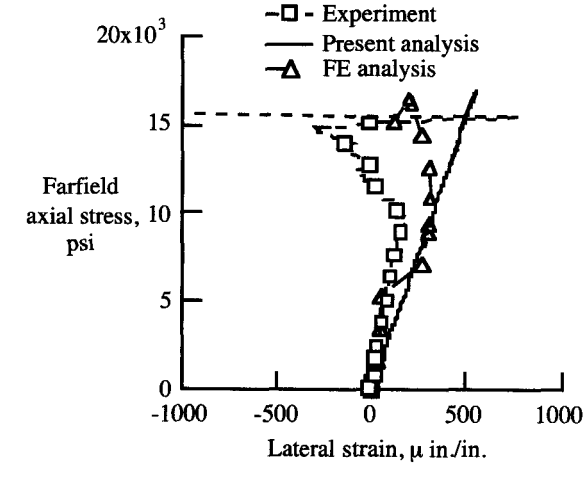

b. Lateral strain results

Figure 11. Continued.

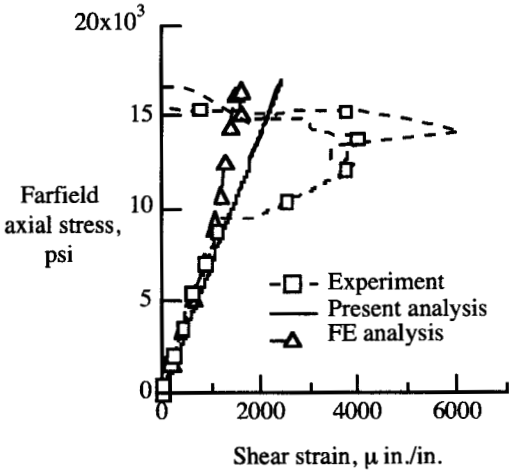

c. Shear strain results

Figure 11. Concluded.